K_S^0 and Λ^0 production studies in $p\bar{p}$ collisions at $\sqrt{s} = 1800$ and 630 GeV

D. Acosta,[14] T. Affolder,[7] M. G. Albrow,[13] D. Ambrose,[36] D. Amidei,[27] K. Anikeev,[26] J. Antos,[1] G. Apollinari,[13] T. Arisawa,[50] A. Artikov,[11] W. Ashmanskas,[2] F. Azfar,[34] P. Azzi-Bacchetta,[35] N. Bacchetta,[35] H. Bachacou,[24] W. Badgett,[13] A. Barbaro-Galtieri,[24] V. E. Barnes,[39] B. A. Barnett,[21] S. Baroiant,[5] M. Barone,[15] G. Bauer,[26] F. Bedeschi,[37] S. Behari,[21] S. Belforte,[47] W. H. Bell,[17] G. Bellettini,[37] J. Bellinger,[51] D. Benjamin,[12] A. Beretvas,[13] A. Bhatti,[41] M. Binkley,[13] D. Bisello,[35] M. Bishai,[13] R. E. Blair,[2] C. Blocker,[4] K. Bloom,[27] B. Blumenfeld,[21] A. Bocci,[41] A. Bodek,[40] G. Bolla,[39] A. Bolshov,[26] D. Bortoletto,[39] J. Boudreau,[38] C. Bromberg,[28] E. Brubaker,[24] J. Budagov,[11] H. S. Budd,[40] K. Burkett,[13] G. Busetto,[35] K. L. Byrum,[2] S. Cabrera,[12] M. Campbell,[27] W. Carithers,[24] D. Carlsmith,[51] A. Castro,[3] D. Cauz,[47] A. Cerri,[24] L. Cerrito,[20] J. Chapman,[27] C. Chen,[36] Y. C. Chen,[1] M. Chertok,[5] G. Chiarelli,[37] G. Chlachidze,[13] F. Chlebana,[13] M. L. Chu,[1] J. Y. Chung,[32] W.-H. Chung,[51] Y. S. Chung,[40] C. I. Ciobanu,[20] A. G. Clark,[16] M. Coca,[40] A. Connolly,[24] M. Convery,[41] J. Conway,[43] M. Cordelli,[15] J. Cranshaw,[45] R. Culbertson,[13] D. Dagenhart,[4] S. D'Auria,[17] P. de Barbaro,[40] S. De Cecco,[42] S. Dell'Agnello,[15] M. Dell'Orso,[37] S. Demers,[40] L. Demortier,[41] M. Deninno,[3] D. De Pedis,[42] P. F. Derwent,[13] C. Dionisi,[42] J. R. Dittmann,[13] A. Dominguez,[24] S. Donati,[37] M. D'Onofrio,[16] T. Dorigo,[35] N. Eddy,[20] R. Erbacher,[13] D. Errede,[20] S. Errede,[20] R. Eusebi,[40] S. Farrington,[17] R. G. Feild,[52] J. P. Fernandez,[39] C. Ferretti,[27] R. D. Field,[14] I. Fiori,[37] B. Flaugher,[13] L. R. Flores-Castillo,[38] G. W. Foster,[13] M. Franklin,[18] J. Friedman,[26] I. Furic,[26] M. Gallinaro,[41] M. Garcia-Sciveres,[24] A. F. Garfinkel,[39] C. Gay,[52] D. W. Gerdes,[27] E. Gerstein,[9] S. Giagu,[42] P. Giannetti,[37] K. Giolo,[39] M. Giordani,[47] P. Giromini,[15] V. Glagolev,[11] D. Glenzinski,[13] M. Gold,[30] N. Goldschmidt,[27] J. Goldstein,[34] G. Gomez,[8] M. Goncharov,[44] I. Gorelov,[30] A. T. Goshaw,[12] Y. Gotra,[38] K. Goulianos,[41] A. Gresele,[3] C. Grosso-Pilcher,[10] M. Guenther,[39] J. Guimaraes da Costa,[18] C. Haber,[24] S. R. Hahn,[13] E. Halkiadakis,[40] R. Handler,[51] F. Happacher,[15] K. Hara,[48] R. M. Harris,[13] F. Hartmann,[22] K. Hatakeyama,[41] J. Hauser,[6] J. Heinrich,[36] M. Hennecke,[22] M. Herndon,[21] C. Hill,[7] A. Hocker,[40] K. D. Hoffman,[10] S. Hou,[1] B. T. Huffman,[34] R. Hughes,[32] J. Huston,[28] J. Incandela,[7] G. Introzzi,[37] M. Iori,[42] C. Issever,[7] A. Ivanov,[40] Y. Iwata,[19] B. Iyutin,[26] E. James,[13] M. Jones,[39] T. Kamon,[44] J. Kang,[27] M. Karagoz Unel,[31] S. Kartal,[13] H. Kasha,[20] Y. Kato,[33] R. D. Kennedy,[13] R. Kephart,[13] B. Kilminster,[40] D. H. Kim,[23] H. S. Kim,[20] M. J. Kim,[9] S. B. Kim,[23] S. H. Kim,[48] T. H. Kim,[26] Y. K. Kim,[10] M. Kirby,[12] L. Kirsch,[4] S. Klimenko,[14] P. Koehn,[32] K. Kondo,[50] J. Konigsberg,[14] A. Korn,[26] A. Korytov,[14] J. Kroll,[36] M. Kruse,[12] V. Krutelyov,[44] S. E. Kuhlmann,[2] N. Kuznetsova,[13] A. T. Laasanen,[39] S. Lami,[41] S. Lammel,[13] J. Lancaster,[12] M. Lancaster,[25] R. Lander,[5] K. Lannon,[32] A. Lath,[43] G. Latino,[30] T. LeCompte,[2] Y. Le,[21] J. Lee,[40] S. W. Lee,[44] N. Leonardo,[26] S. Leone,[37] J. D. Lewis,[13] K. Li,[52] C. S. Lin,[13] M. Lindgren,[6] T. M. Liss,[20] D. O. Litvintsev,[13] T. Liu,[13] N. S. Lockyer,[36] A. Loginov,[29] M. Loreti,[35] D. Lucchesi,[35] P. Lukens,[13] L. Lyons,[34] J. Lys,[24] R. Madrak,[18] K. Maeshima,[13] P. Maksimovic,[21] L. Malferrari,[3] M. Mangano,[37] G. Manca,[34] M. Mariotti,[35] M. Martin,[21] A. Martin,[52] V. Martin,[31] M. Martínez,[13] P. Mazzanti,[3] K. S. McFarland,[40] P. McIntyre,[44] M. Menguzzato,[35] A. Menzione,[37] P. Merkel,[13] C. Mesropian,[41] A. Meyer,[13] T. Miao,[13] J. S. Miller,[27] R. Miller,[28] S. Miscetti,[15] G. Mitselmakher,[14] N. Moggi,[3] R. Moore,[13] T. Moulik,[39] A. Mukherjee,[13] M. Mulhearn,[26] T. Muller,[22] A. Munar,[36] P. Murat,[13] J. Nachtman,[13] S. Nahn,[52] I. Nakano,[19] R. Napora,[21] C. Nelson,[13] T. Nelson,[13] C. Neu,[32] M. S. Neubauer,[26] C. Newman-Holmes,[13] F. Niell,[27] T. Nigmanov,[38] L. Nodulman,[2] S. H. Oh,[12] Y. D. Oh,[23] T. Ohsugi,[19] T. Okusawa,[33] W. Orejudos,[24] C. Pagliarone,[37] F. Palmonari,[37] R. Paoletti,[37] V. Papadimitriou,[45] J. Patrick,[13] G. Pauletta,[47] M. Paulini,[9] T. Pauly,[34] C. Paus,[26] D. Pellett,[5] A. Penzo,[47] T. J. Phillips,[12] G. Piacentino,[37] J. Piedra,[8] K. T. Pitts,[20] A. Pompoš,[39] L. Pondrom,[51] G. Pope,[38] O. Poukov,[11] T. Pratt,[34] F. Prokoshin,[11] J. Proudfoot,[2] F. Ptohos,[15] G. Punzi,[37] J. Rademacker,[34] A. Rakitine,[26] F. Ratnikov,[43] H. Ray,[27] A. Reichold,[34] P. Renton,[34] M. Rescigno,[42] F. Rimondi,[3] L. Ristori,[37] W. J. Robertson,[12] T. Rodrigo,[8] S. Rolli,[49] L. Rosenson,[26] R. Roser,[13] R. Rossin,[35] C. Rott,[39] A. Roy,[39] A. Ruiz,[8] D. Ryan,[49] A. Safonov,[5] R. St. Denis,[17] W. K. Sakumoto,[40] D. Saltzberg,[6] C. Sanchez,[32] A. Sansoni,[15] L. Santi,[47] S. Sarkar,[42] P. Savard,[46] A. Savoy-Navarro,[13] P. Schlabach,[13] E. E. Schmidt,[13] M. P. Schmidt,[52] M. Schmitt,[31] L. Scodellaro,[35] A. Scribano,[37] A. Sedov,[39] S. Seidel,[30] Y. Seiya,[48] A. Semenov,[11] F. Semeria,[3] M. D. Shapiro,[24] P. F. Shepard,[38] T. Shibayama,[48] M. Shimojima,[48] M. Shochet,[10] A. Sidoti,[35] A. Sill,[45] P. Sinervo,[46] A. J. Slaughter,[52] K. Sliwa,[49] F. D. Snider,[13] R. Snihur,[25] M. Spezziga,[45] L. Spiegel,[13] F. Spinella,[37] M. Spiropulu,[7] A. Stefanini,[37] J. Strologas,[30] D. Stuart,[7] A. Sukhanov,[14] K. Sumorok,[26] T. Suzuki,[48] R. Takashima,[19] K. Takikawa,[48] M. Tanaka,[2] M. Tecchio,[27] P. K. Teng,[1] K. Terashi,[41] R. J. Tesarek,[13] S. Tether,[26] J. Thom,[13] A. S. Thompson,[17] E. Thomson,[32] P. Tipton,[40] S. Tkaczyk,[13] D. Toback,[44] K. Tollefson,[28] D. Tonelli,[37] M. Tönnesmann,[28] H. Toyoda,[33] W. Trischuk,[46] J. Tseng,[26] D. Tsybychev,[14] N. Turini,[37] F. Ukegawa,[48] T. Unverhau,[17] T. Vaiciulis,[40] A. Varganov,[27] E. Vataga,[37] S. Vejcik III,[13] G. Velev,[13] G. Veramendi,[24] R. Vidal,[13] I. Vila,[8] R. Vilar,[8] I. Volobouev,[24] M. von der Mey,[6] R. G. Wagner,[2] R. L. Wagner,[13] W. Wagner,[22] Z. Wan,[43] C. Wang,[12] M. J. Wang,[1] S. M. Wang,[14]

B. Ward,[17] S. Waschke,[17] D. Waters,[25] T. Watts,[43] M. Weber,[24] W. C. Wester III,[13] B. Whitehouse,[49] A. B Wicklund,[2] E. Wicklund,[13] H. H. Williams,[36] P. Wilson,[13] B. L. Winer,[32] S. Wolbers,[13] M. Wolter,[49] S. Worm,[43] X. Wu,[16] F. Würthwein,[26] U. K. Yang,[10] W. Yao,[24] G. P. Yeh,[13] K. Yi,[21] J. Yoh,[13] T. Yoshida,[33] I. Yu,[23] S. Yu,[36] J. C. Yun,[13] L. Zanello,[42] A. Zanetti,[47] F. Zetti,[24] and S. Zucchelli[3]

(CDF Collaboration)

[1]*Institute of Physics, Academia Sinica, Taipei, Taiwan 11529, Republic of China*
[2]*Argonne National Laboratory, Argonne, Illinois 60439, USA*
[3]*Istituto Nazionale di Fisica Nucleare, University of Bologna, I-40127 Bologna, Italy*
[4]*Brandeis University, Waltham, Massachusetts 02254, USA*
[5]*University of California at Davis, Davis, California 95616, USA*
[6]*University of California at Los Angeles, Los Angeles, California 90024, USA*
[7]*University of California at Santa Barbara, Santa Barbara, California 93106, USA*
[8]*Instituto de Fisica de Cantabria, CSIC-University of Cantabria, 39005 Santander, Spain*
[9]*Carnegie Mellon University, Pittsburgh, Pennsylvania 15213*
[10]*Enrico Fermi Institute, University of Chicago, Chicago, Illinois 60637, USA*
[11]*Joint Institute for Nuclear Research, RU-141980 Dubna, Russia*
[12]*Duke University, Durham, North Carolina 27708, USA*
[13]*Fermi National Accelerator Laboratory, Batavia, Illinois 60510, USA*
[14]*University of Florida, Gainesville, Florida 32611, USA*
[15]*Laboratori Nazionali di Frascati, Istituto Nazionale di Fisica Nucleare, I-00044 Frascati, Italy*
[16]*University of Geneva, CH-1211 Geneva 4, Switzerland*
[17]*Glasgow University, Glasgow G12 8QQ, United Kingdom*
[18]*Harvard University, Cambridge, Massachusetts 02138, USA*
[19]*Hiroshima University, Higashi-Hiroshima 724, Japan*
[20]*University of Illinois, Urbana, Illinois 61801, USA*
[21]*The Johns Hopkins University, Baltimore, Maryland 21218, USA*
[22]*Institut für Experimentelle Kernphysik, Universität Karlsruhe, 76128 Karlsruhe, Germany*
[23]*Center for High Energy Physics: Kyungpook National University, Taegu 702-701; Seoul National University, Seoul 151-742; and SungKyunKwan University, Suwon 440-746; Korea*
[24]*Ernest Orlando Lawrence Berkeley National Laboratory, Berkeley, California 94720, USA*
[25]*University College London, London WC1E 6BT, United Kingdom*
[26]*Massachusetts Institute of Technology, Cambridge, Massachusetts 02139, USA*
[27]*University of Michigan, Ann Arbor, Michigan 48109, USA*
[28]*Michigan State University, East Lansing, Michigan 48824, USA*
[29]*Institution for Theoretical and Experimental Physics, ITEP, Moscow 117259, Russia*
[30]*University of New Mexico, Albuquerque, New Mexico 87131, USA*
[31]*Northwestern University, Evanston, Illinois 60208, USA*
[32]*The Ohio State University, Columbus, Ohio 43210, USA*
[33]*Osaka City University, Osaka 588, Japan*
[34]*University of Oxford, Oxford OX1 3RH, United Kingdom*
[35]*Universita di Padova, Istituto Nazionale di Fisica Nucleare, Sezione di Padova, I-35131 Padova, Italy*
[36]*University of Pennsylvania, Philadelphia, Pennsylvania 19104, USA*
[37]*Istituto Nazionale di Fisica Nucleare, University and Scuola Normale Superiore of Pisa, I-56100 Pisa, Italy*
[38]*University of Pittsburgh, Pittsburgh, Pennsylvania 15260, USA*
[39]*Purdue University, West Lafayette, Indiana 47907, USA*
[40]*University of Rochester, Rochester, New York 14627, USA*
[41]*Rockefeller University, New York, New York 10021, USA*
[42]*Instituto Nazionale de Fisica Nucleare, Sezione di Roma, University di Roma I, "La Sapienza," I-00185 Roma, Italy*
[43]*Rutgers University, Piscataway, New Jersey 08855, USA*
[44]*Texas A&M University, College Station, Texas 77843, USA*
[45]*Texas Tech University, Lubbock, Texas 79409, USA*
[46]*Institute of Particle Physics, University of Toronto, Toronto M5S 1A7, Canada*
[47]*Istituto Nazionale di Fisica Nucleare, University of Trieste/Udine, Italy*
[48]*University of Tsukuba, Tsukuba, Ibaraki 305, Japan*
[49]*Tufts University, Medford, Massachusetts 02155, USA*
[50]*Waseda University, Tokyo 169, Japan*
[51]*University of Wisconsin, Madison, Wisconsin 53706, USA*
[52]*Yale University, New Haven, Connecticut 06520, USA*

(Received 28 April 2005; published 7 September 2005)

We present a study of the production of K^0_S and Λ^0 in inelastic $p\bar{p}$ collisions at $\sqrt{s} = 1800$ and 630 GeV using data collected by the CDF experiment at the Fermilab Tevatron. Analyses of K^0_S and Λ^0 multiplicity and transverse momentum distributions, as well as of the dependencies of the average number and $\langle p_T \rangle$ of K^0_S and Λ^0 on charged particle multiplicity, are reported. Systematic comparisons are performed for the full sample of inelastic collisions, and for the low and high momentum transfer subsamples, at the two energies. The p_T distributions extend above 8 GeV/c, showing a $\langle p_T \rangle$ higher than previous measurements. The dependence of the mean $K^0_S(\Lambda^0)$ p_T on the charged particle multiplicity for the three samples shows a behavior analogous to that of charged primary tracks.

DOI: 10.1103/PhysRevD.72.052001 PACS numbers: 13.85.Hd, 13.85.Ni, 13.87.Fh

I. INTRODUCTION

Hadron interactions are often classified as either ''hard'' or ''soft'' [1,2]. Although there is not any formal definition for either, the term ''hard interactions'' denotes high momentum transfer parton-parton interactions typically associated with such phenomena as jets of high energy transverse to the incoming hadron momenta (E_T). The soft interaction component encompasses everything else and dominates the inelastic cross section. From a theoretical point of view, perturbative QCD provides a reasonable description of high-E_T jet production. However, nonperturbative QCD, relevant to low-E_T hadronic production, is not well understood. Some QCD-inspired models [2] attempt to describe these processes by the superposition of many parton interactions extrapolated to very low momentum transfers. It is not known, however, if these or other collective multiparton processes are at work. The experimental studies of low-E_T interactions are usually performed on data collected using minimum bias (MB) triggers, which, ideally, sample events in fixed proportion to the production rate—in other words, in their ''natural'' distribution. Lacking a comprehensive description of the microscopic processes [3] involved in low-E_T interactions, our knowledge of the details of low transverse momentum (p_T) particle production rests largely upon empirical connections between phenomenological models and data collected with MB triggers at many center-of-mass energies ($E_{\rm cms}$). Such comparisons necessarily face the difficulty of isolating events of a purely soft or hard nature.

Comparative studies of the event structure through collective variables such as the charged particle multiplicity and the transverse energy of the event are important to our understanding of the soft production mechanism. In a previous paper [4], a novel approach in addressing this issue using samples of $p\bar{p}$ collisions at $\sqrt{s} = 1800$ and 630 GeV collected with a MB trigger was described. The analysis divided the full MB samples into two subsamples, one highly enriched in soft interactions, the other in hard interactions. Comparisons between the subsamples and as a function of $E_{\rm cms}$ were performed. The same approach has been applied here to the production of strange particles.

Beside gluons and the lighter quarks u and d, strange quark production is the only component of low-p_T multiparticle interactions which is statistically significant and experimentally accessible with a MB trigger. It is also a probe for investigating the transition of soft hadron interactions to the QCD high-p_T perturbative region.

This paper describes a study of K^0_S and Λ^0 production in $p\bar{p}$ interactions at different $E_{\rm cms}$. Inclusive distributions of the multiplicity and transverse momentum of K^0_S and Λ^0 are presented first. The high statistics of the data sample collected at $\sqrt{s} = 1800$ and 630 GeV allow an extension of the range and precision of these measurements with respect to previous ones. Studies of the dependence of the average p_T of $K^0_S(\Lambda^0)$ and of their mean number on the event charged multiplicity are also presented. Different behavior of the hard and soft subsamples is observed, consistent with prior reports on charged particles [4].

II. DATA COLLECTION

A. The CDF detector

Data samples have been collected with the CDF detector at the Fermilab Tevatron Collider. The CDF apparatus has been described elsewhere [5]; here only the parts of the detector utilized for the present analysis are discussed. The coordinate system is defined with respect to the proton beam direction, which defines the positive z direction, while the azimuthal angle ϕ is measured around the beam axis. The polar angle θ is measured with respect to the positive z direction. The pseudorapidity, η, is often used and is defined as $\eta = -\ln(\tan[\theta/2])$. Transverse components of particle energy and momentum are conventionally defined as projections onto the plane transverse to the beam line, $E_T = E\sin\theta$ and $p_T = |\vec{p}|\sin\theta$.

Data were collected with a MB trigger at 1800 GeV during runs 1A (1992–93) and 1B (1994–95), and at 1800 and 630 GeV during run 1C (1995–96). This trigger requires coincident hits in scintillator counters, located at 5.8 m from either side downstream of the nominal interaction point and covering the pseudorapidity interval $3.2 < |\eta| < 5.9$, in coincidence with a beam crossing.

The analysis uses charged tracks reconstructed within the central tracking chamber (CTC). The CTC is a cylindrical drift chamber covering an η interval of about three units with high efficiency for $|\eta| \leq 1$ and $p_T \geq 0.4$ GeV/c. The inner radius of the CTC is 31.0 cm and the outer radius is 132.5 cm. The full CTC volume is contained in a superconducting solenoidal magnet which

operates at 1.4 T [6]. The CTC has 84 sampling wire layers, organized into 5 axial and 4 stereo ''superlayers'' [7]. Axial superlayers have 12 radially separated layers of sense wires, parallel to the z axis (the beam axis), that measure the r-ϕ position of a track. Stereo superlayers have 6 sense wire layers, with a $\sim 3^\circ$ stereo angle, which measure a combination of r-ϕ and z positions. The stereo angle direction alternates with each neighboring stereo superlayer. Measurements from axial and stereo superlayers are combined to form a three-dimensional track. The spatial resolution of each point measurement in the CTC is less than 200 μm; the transverse momentum resolution, including multiple-scattering effects, is $\sigma_{p_T}/p_T^2 \leq 0.003\ (\mathrm{GeV}/c)^{-1}$.

Inside the CTC inner radius, a set of time-projection chambers (VTX) [8] provides r-z tracking information out to a radius of 22 cm for $|\eta| < 3.25$. The VTX is used in this analysis to find the z positions of event vertices, defined as sets of tracks converging to the same point along the z axis. The closest detector to the beam pipe is the silicon vertex finder (SVX), used to reconstruct vertex positions in the transverse view. Reconstructed vertices are classified as either ''primary'' or ''secondary'' based upon several parameters: a minimum of 4 converging track segments in $|\eta| < 3$ (a track segment is a sequence of 4 aligned hits), the total number of hits used to form a segment, forward-backward symmetry, and vertex isolation. Isolated, higher multiplicity vertices with highly symmetric topologies are typically classified as primary; lower multiplicity, highly asymmetric vertices, or those with few hits in the reconstructed tracks, are typically classified as secondary. Systematic uncertainties introduced by the vertex classification scheme are discussed in Sec. VI.

The transverse energy flux is measured by a calorimeter system [9] covering $|\eta| \leq 4.2$. The calorimeter consists of three subsystems, each with separate electromagnetic and hadronic components: the central calorimeter, covering the range $|\eta| < 1.1$; the end plug, covering $1.1 < |\eta| < 2.4$; and the forward calorimeter, covering $2.2 < |\eta| < 4.2$. Energy measurements are made within projective ''towers'' that span 0.1 units of η and 15° (5°) in ϕ within the central (end plug and forward) calorimeter.

B. The data set

The 1800 GeV MB data sample consists of subsamples collected during three different time periods. Approximately 1.7×10^6 events were collected in run 1A at an average luminosity of $3.3 \times 10^{30}\ \mathrm{s}^{-1}\mathrm{cm}^{-2}$, 1.5×10^6 in run 1B at an average luminosity of $9.1 \times 10^{30}\ \mathrm{s}^{-1}\mathrm{cm}^{-2}$, and 1.06×10^5 in run 1C at an average luminosity of $9.0 \times 10^{30}\ \mathrm{s}^{-1}\mathrm{cm}^{-2}$. The 630 GeV data set consists of about 2.6×10^6 events recorded during run 1C at an average luminosity of $1.3 \times 10^{30}\ \mathrm{s}^{-1}\mathrm{cm}^{-2}$.

Additional event selection conducted offline removed the following events: (i) events identified as containing cosmic ray particles as determined by time-of-flight measurements using scintillator counters in the central calorimeter; (ii) events with no reconstructed tracks; (iii) events exhibiting symptoms of known calorimeter problems; (iv) events with at least one charged particle reconstructed in the CTC to have $p_T \geq 400\ \mathrm{MeV}/c$, but no central calorimeter tower with energy deposition above 100 MeV; (v) events with more than one primary vertex; (vi) events with a primary vertex more than 60 cm away from the center of the detector (in order to ensure uniform acceptance in the assumed fiducial region and good track and calorimeter energy reconstruction); and (vii) events with no primary vertices.

After all event selection requirements, 2 079 558 events remain in the full MB sample at $\sqrt{s} = 1800$ GeV and 1 963 157 at $\sqrt{s} = 630$ GeV. The vast majority of rejected events failed the vertex selection. About 0.01% of selected events contain background tracks from cosmic rays that are coincident in time with the beam crossing and pass near the event vertex. The residual contamination due to the interactions of the beam particles with the gas in the beam pipe is about 0.02%. A more detailed discussion of the systematic uncertainties arising from the event selection criteria and other sources is presented in Ref. [4].

III. CHARGED TRACKS AND $K_S^0(\Lambda^0)$ SELECTION

We require all reconstructed tracks to pass through a minimum number of layers in the CTC and have a minimum number of hits in each superlayer in order to reduce the number of misreconstructed tracks and those with large reconstruction uncertainties. The remaining track set, which includes primary and secondary tracks, is used as a starting point for both the selection of primary charged tracks and for the $K_S^0(\Lambda^0)$ candidate identification procedure.

Charged-track multiplicity definition.—Tracks are required to pass within 0.5 cm of the beam axis, and within 5 cm along the z axis from the primary event vertex. In order to ensure high efficiency and acceptance, tracks are accepted only if they satisfy the conditions $p_T \geq 0.4\ \mathrm{GeV}/c$ and $|\eta| \leq 1.0$. This selection defines the charged-track multiplicity in an event, $N_{\mathrm{ch}}^{\star}$.

K_S^0 and Λ^0 selection.—K_S^0 and Λ^0 [10] (from now on collectively referred to as V^0) are selected looking for opposite-charge pairs of tracks converging to a common vertex displaced from the beam line in the transverse direction. A vertex fit is performed to ensure that the two tracks originate from the same vertex. A candidate is required to have a fit probability greater than 5%. In a further step a fit is performed constraining the V^0 momentum vector (within the track uncertainties) to point in the direction of the primary vertex (pointing constraint fit). The candidates are kept if the fit probability is greater than 5% and the recomputed invariant mass is within 3 standard deviations of the world average K_S^0 or Λ^0 mass [11].

TABLE I. Raw and corrected numbers of K^0_S and Λ^0 found in each data set. In the rightmost three columns the fraction of $K^0_S(\Lambda^0)$ per event is shown. The uncertainties on all the corrected numbers and fraction of $K^0_S(\Lambda^0)$ per event include the systematic uncertainty. The total number of MB events at $\sqrt{s} = 1800$ GeV (630 GeV) is 2 079 558 (1 963 157).

		RAW			CORRECTED			FRACTION of $K^0_S(\Lambda^0)$/EVENT (%)		
		MB	Soft	Hard	MB ($\times 10^3$)	Soft ($\times 10^3$)	Hard ($\times 10^3$)	MB	Soft	Hard
1800 GeV	K^0_S	36642	6733	29909	180 ± 50	34 ± 10	150 ± 40	8.8 ± 2.6	3.5 ± 1.0	13.3 ± 4.0
	Λ^0	7518	782	6736	90 ± 30	9 ± 3	80 ± 20	4.3 ± 1.0	1.0 ± 0.3	7.2 ± 2.2
630 GeV	K^0_S	32222	9835	22387	170 ± 50	50 ± 15	120 ± 35	8.6 ± 2.6	4.5 ± 1.4	14.3 ± 4.3
	Λ^0	5883	1098	4785	70 ± 20	13 ± 4	60 ± 20	3.7 ± 1.1	1.2 ± 0.4	7.1 ± 2.1

The analysis selection also requires:

(i) $L_{xy}(V^0) \geq 1$ cm, where L_{xy} is the distance from the primary vertex to the decay vertex of the V^0 in the r-ϕ plane;
(ii) both decay tracks have $|\eta| \leq 1.5$ and $p_T \geq 0.3$ GeV/c;
(iii) the V^0 line-of-flight is close to the event vertex along the z axis: $|z_0^{V^0} - z_0^{\text{vertex}}| < 6$ cm;
(iv) impact parameter $d_0(V^0) < 0.7$ cm;
(v) $p_T(V^0) \geq 0.4$ GeV/c and $|\eta(V^0)| \leq 1.0$.

For events with more than one V^0 candidate sharing the same track, only the candidate with the lower vertex fit $\chi^2/N_{\text{d.o.f.}}$ is retained.

After all selection requirements, we find 36 642 K^0_S and 7518 Λ^0 in the 1800 GeV MB sample and 32 222 K^0_S and 5883 Λ^0 in the 630 GeV MB sample (see Table I).

The invariant mass distributions of the K^0_S and Λ^0 surviving the selection requirements, but with the mass window extended to 10 standard deviations from the world average, are shown in Fig. 1; in both cases the peaks are narrow but, because of the fit procedure, the background is not flat and may not be accounted for by the level of the sidebands. We also note that this background includes the contamination of K^0_S in the Λ^0 sample and vice versa. A detailed background evaluation is discussed in Sec. V.

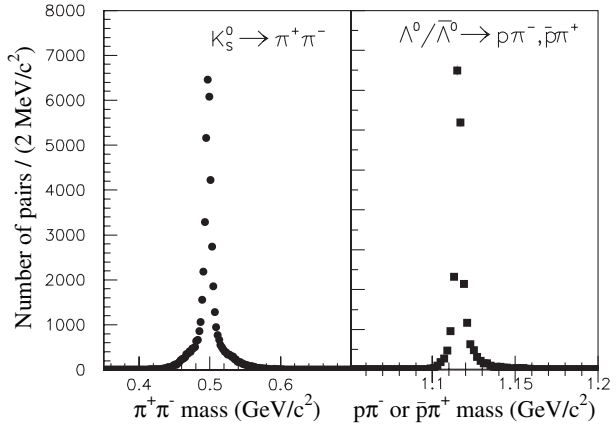

FIG. 1. Invariant mass with a π-π and π-p mass assignment for oppositely signed track pairs passing all selection requirements but allowing the mass to be within 10σ from the nominal mass. The background includes the contamination by K^0_S in the Λ^0 sample and vice versa. 1800 GeV data are shown.

IV. SELECTION OF *SOFT* AND *HARD* INTERACTIONS

The identification of soft and hard interactions is largely a matter of definition [12] since it is unknown how to distinguish soft and hard parton interactions. This is true from both the theoretical and experimental points of view. In this analysis, we use a jet reconstruction algorithm to define the two cases. The algorithm employs a cone with radius $R = (\Delta\eta^2 + \Delta\phi^2)^{1/2} = 0.7$ to define "clusters" of calorimeter towers belonging to a jet. To be considered, a cluster must have a transverse energy E_T, defined as the scalar sum of the transverse energy of all the towers included in the cone, of at least 1 GeV in a seed tower, plus at least 0.1 GeV in an adjacent tower.

In the regions $|\eta| < 0.02$ and $1.1 < |\eta| < 1.2$, a track-clustering algorithm is used instead of the calorimeter algorithm to compensate for energy lost in calorimeter cracks. A track cluster is defined as one track with $p_T > 0.7$ GeV/c and at least one other track with $p_T \geq 0.4$ GeV/c in a cone of radius $R = 0.7$.

We define a *soft* event as one that contains no cluster with $E_T > 1.1$ GeV. All other events are classified as *hard*.

V. EFFICIENCY AND CORRECTIONS

The probability of observing a real V^0 in the apparatus is influenced by several effects. In this section we discuss the efficiency of track reconstruction, the correction for limited acceptance, and evaluation of the background. At the end, some cross-checks of the correction procedures are also briefly described.

1. The efficiency for finding $K^0_S(\Lambda^0)$ has been investigated in two different ways. In the first method, simulated hits from singly generated V^0 are embedded among the set of hits of MB events from the data. The events are then reconstructed with standard V^0 search and selection. In the second method, entire MB events with V^0 production and decay are generated with PYTHIA/JETSET Monte Carlo (MC) [4,13]. Full CDF detector simulation and reconstruction are then applied to the events and the resulting reconstructed kinematic distributions are similar to those

observed in the data. The results from the two methods are compatible within the statistical uncertainties.

The efficiency is defined as the ratio of the reconstructed to the generated number of V^0 in the fiducial region. It is examined as a function of single kinematical variables of the V^0, integrating over all the remaining variables. The embedding method, given its almost flat V^0 distribution in all variables, gives smooth and statistically better determined efficiency dependences from all observables over all the acceptance limits. The results of this method are used to determine the shape of the efficiency as a function of any chosen variable. Each efficiency distribution from the embedding method is then scaled by an overall normalization factor so that the integrated efficiency obtained from the embedding method matches the integrated efficiency from the full MC method.

The efficiency for finding a single $K^0_S(\Lambda^0)$ is approximately constant [around 40% (32%)] as a function of $\eta(V^0)$ in the region of $|\eta(V^0)| < 1$ and $p_T(V^0) > 0.4$ GeV/c. As a function of $p_T(V^0)$ (in the same η region), the efficiency rises rapidly from 25% (15%) at 0.4 GeV/c to about 50% (40%) for $p_T \sim 1$ GeV/c, and then slowly decreases to $\simeq 20\%$ ($\simeq 15\%$) for $p_T \gtrsim 8$ GeV/c. This behavior is due to the difficulty in reconstructing low-p_T secondary tracks and in identifying secondary vertices far from the primary vertex. The efficiency also diminishes for $L_{xy} \lesssim 3$ cm, while it is roughly constant as a function of the charged multiplicity of the event. The overall efficiency is about 39% for K^0_S and 31% for Λ^0.

2. A correction for the fiducial acceptance requirement in L_{xy} and in the p_T of the $K^0_S(\Lambda^0)$ decay products is estimated using MC and found to range from about 15 (20) at $p_T = 0.5(1)$ GeV/c to about 1 for $p_T \gtrsim 5$ GeV/c.

3. The contamination by Λ^0 in the K^0_S sample is estimated to be $\simeq 3\%$ as found in the PYTHIA MC simulation; the contamination by K^0_S in the Λ^0 sample is about 7% on average while it is almost 50% for $p_T(\Lambda^0) < 1.5$ GeV/c. The same MC sample is used to compute the probability of selecting fake secondary vertices (not due to K^0_S or Λ^0 decays). Such probability is found to account for roughly 25% of the K^0_S and 40% of the Λ^0.

4. The overall correction factor for a generic inclusive variable X [e.g. the $p_T(V^0)$] is given by the expression

$$C(X) = \frac{1 - R_{\rm fake}(X)}{\epsilon(X) \times A(X)} \tag{1}$$

where $R_{\rm fake}$ is the probability of a fake V^0, ϵ is the global efficiency, and A is the acceptance. The overall correction factors, as a function of $p_T(V^0)$, are shown in Fig. 2. The integrated MC correction factors are estimated to be 4.5 ± 0.1 and 10.1 ± 0.2 for K^0_S and Λ^0, respectively.

5. Because of the small differences that exist between some PYTHIA distributions and the data, we expect that the MC correction will not be fully reliable in the regions where it changes very rapidly. Evidence of this is given by the reconstructed V^0 p_T versus the proper time which shows a depletion in the low-p_T and low-lifetime region, even after applying the MC correction.

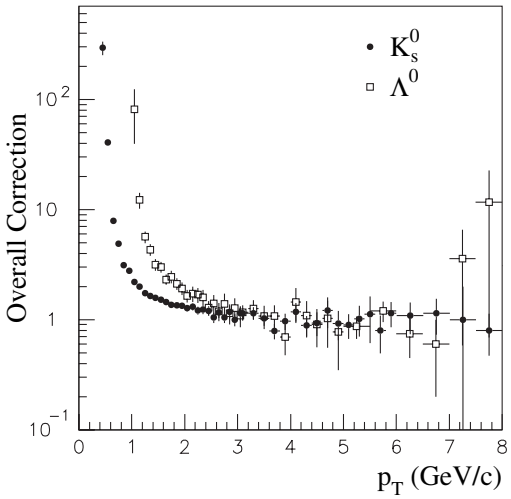

FIG. 2. Overall correction factors at 1800 GeV for $K^0_S(\Lambda^0)$ as a function of the transverse momentum. The correction factors are defined in the text.

We use the following method to correct the counted number of $K^0_S(\Lambda^0)$ in this region. The $K^0_S(\Lambda^0)$ invariant p_T distributions for the full MB sample are fitted with a functional power-law form:

$$E\frac{d^3N_{V^0}}{dp^3} = A\left(\frac{p_0}{p_0 + p_T}\right)^n, \tag{2}$$

where E is the particle energy and p_0, A, and n are free parameters, in the region above 0.8 GeV/c (1.1 GeV/c for Λ^0). This equation has been widely used to fit the p_T distributions of charged tracks down to the lower measured p_T [14]. The fitted function is extrapolated down to $p_T(V^0) = 0.4$ GeV/c and the corrected number of $K^0_S(\Lambda^0)$ is extracted from the integral of the curve.

In the full MB sample, the number of undetected V^0 is estimated to be approximately 18×10^3 K^0_S and 14×10^3 Λ^0 at 1800 GeV, and 24×10^3 and 12×10^3, respectively, at 630 GeV.

6. The above correction affects the measurements of the mean number of V^0 per event and of the mean p_T when computed at fixed $N^\star_{\rm ch}$. The latter is calculated as the sum of the p_T's of $K^0_S(\Lambda^0)$, above 0.4 GeV/c, observed in events of a given charged multiplicity, divided by the number of $K^0_S(\Lambda^0)$:

$$\langle p_T \rangle = \frac{1}{N_{V^0}} \sum_i^{N_{V^0}} p_{T_i}. \tag{3}$$

An estimate of the number of undetected V^0 and the resulting effect on the $\langle p_T(V^0) \rangle$ and on the V^0 multiplicity are obtained, for each $p_T(V^0)$ distribution, with the procedure used in the inclusive case. The constraint that the sum

of undetected V^0 for each multiplicity should give the number of undetected V^0 computed from the inclusive p_T distribution is imposed. The corrected $\langle p_T(V^0)\rangle$ is computed by extrapolating the fitted $p_T(V^0)$ distribution down to $p_T(V^0) = 0.4$ GeV/c.

7. The consistency of the correction procedures described above has been verified through the following cross-checks.

In order to check the selection requirements and the quality of the efficiency correction, the raw and corrected proper lifetime distributions at 1800 GeV are shown in Fig. 3. Fitting to an exponential form gives a K^0_S mean proper lifetime of $(0.89 \pm 0.01) \times 10^{-10}$ s($\chi^2/N_{\text{d.o.f.}} = 49.7/59$) for 1800 GeV and $(0.90 \pm 0.01) \times 10^{-10}$ s($\chi^2/N_{\text{d.o.f.}} = 60.6/56$) for 630 GeV. Both values are consistent with the world average values [11]. The same fit to the Λ^0 proper lifetime distributions gives a mean of $(2.61 \pm 0.07) \times 10^{-10}$ s($\chi^2/N_{\text{d.o.f.}} = 44.2/49$) for 1800 GeV and $(2.61 \pm 0.07) \times 10^{-10}$ s($\chi^2/N_{\text{d.o.f.}} = 57.4/50$) for 630 GeV. The proper lifetime regions used for the fit are $\tau > 0.7 \times 10^{-10}$ s (K^0_S) and $\tau > 10^{-10}$ s (Λ^0).

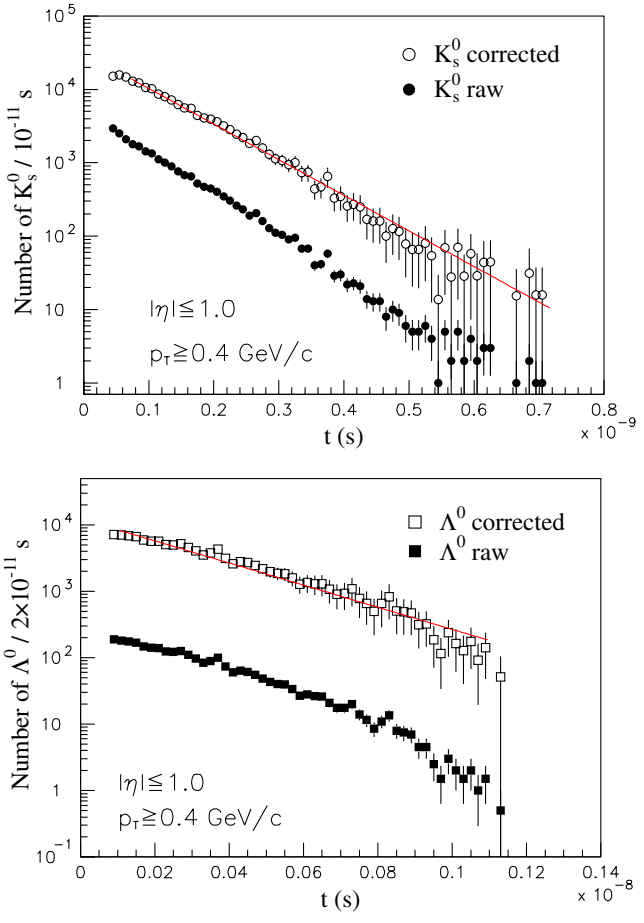

FIG. 3 (color online). Raw and corrected K^0_S and Λ^0 proper lifetime distributions for 1800 GeV data. The line represents the best exponential fit to the data.

The number of undetected V^0 extracted from the fitted p_T curve is also checked. The proper lifetime distributions of Fig. 3 are fitted to an exponential form with fixed slope (the K^0_s/Λ^0 mean lifetimes [11], $\tau_{K^0_s} = 0.8935 \times 10^{-10}$ s; $\tau_{\Lambda^0} = 2.632 \times 10^{-10}$ s) in the region $\tau > 0.7 \times 10^{-10}$ s ($\tau > 10^{-10}$ s for Λ^0) and the fitted curves are integrated down to $\tau = 0$. The number of undetected $K^0_S(\Lambda^0)$ obtained matches to 15% (30%) with the number from the p_T distribution. Furthermore the p_T distributions of $K^0_S(\Lambda^0)$ with proper lifetimes greater than 0.8×10^{-10} s (1.0×10^{-10} s for Λ^0) are compared with the corresponding distributions for all lifetimes; the comparison gives the same values of average p_T. When normalized to one another, the curves give a comparable number of $K^0_S(\Lambda^0)$ in the extrapolated region.

An additional cross-check for correcting the average p_T of the V^0 observed in events of fixed multiplicity consists of plotting the proper lifetime distribution in slices of p_T so that each distribution corresponds to one bin in p_T. This is done for each bin in multiplicity. After fitting the distribution in the long lifetime region in each p_T bin, the correct number of K^0_S in the short lifetime region can be extrapolated from the fits. The $\langle p_T(V^0)\rangle$ can then be recomputed from the modified p_T distribution. The p_T values obtained using the two different correction methods are consistent. In the case of Λ^0, no events are found with p_T below 1 GeV/c due to the tight fiducial requirements imposed in the analysis. Therefore, in the Λ^0 case, the correction method based on extrapolating the proper lifetime distribution at each p_T bin cannot be used. Because of this, the cross-checks are limited to comparing the number of extrapolated Λ^0 in the p_T and proper lifetime distributions of the full data sample.

Finally, we refer to [4] for a detailed discussion of the charged-track selection and reconstruction efficiencies.

VI. SYSTEMATIC UNCERTAINTIES

The two dominant systematic uncertainties come from the acceptance and efficiency correction procedures. As described in Sec. V, acceptance and efficiency corrections have been computed using MC simulation, with an additional correction applied to compensate for MC deficiencies in the low-p_T region between 0.4 and 0.8 GeV/c. The two correction procedures are largely independent, which allows us to evaluate the systematic uncertainties from these two sources separately. The details are described below.

1. We study the sensitivity of this measurement to the differences between the MC predictions and the shapes of the observed V^0 kinematical distributions. We use the following two sets of MC events. The first is created using the default PYTHIA MC. The second is the one used for efficiency studies using the embedding procedure: the V^0's in this set have nonphysical distributions roughly uniform in p_T but not in η. The different correction factors eval-

uated from the above data sets are applied to the measured distributions. Half the difference between the corrected distributions is taken as the systematic uncertainty on the distributions themselves, which amounts to about 10% for the K^0_S and Λ^0 p_T distributions, roughly constant over the whole spectrum.

The effect on the mean p_T value is 3% for K^0_S and 4% for Λ^0. For the K^0_S and Λ^0 multiplicity distributions, the systematic variation ranges from 10% to ~25%. As a function of $N^{\star}_{\rm ch}$, the systematic uncertainty on the number of K^0_S ranges from a few percent to roughly 20% at the highest charged multiplicities.

2. The systematic uncertainty due to the correction for the undetected V^0 in the p_T region between 0.4 and 0.8 GeV/c has been evaluated in the following way. The procedure defined in Sec. V, point 7, is repeated using p_T and proper lifetime distributions both corrected with PYTHIA MC and with the embedding-based correction. The total number of V^0 is computed by integrating the corrected p_T and lifetime spectra for each of the two cases. We end up with four different evaluations of the number of undetected V^0. By comparing the numbers obtained from all combinations, we observe that the largest difference amounts to about 50% of the correction value. This number is taken as the systematic uncertainty on this correction and is counted as a contribution to the systematics on the total number of measured $K^0_S(\Lambda^0)$.

The mean p_T values at fixed multiplicities are also affected by the correction for the undetected $K^0_S(\Lambda^0)$ in the low-p_T region. The systematic uncertainty on the correction is estimated as follows. First it has been verified that the mean p_T after correction is independent of the $K^0_S(\Lambda^0)$ proper lifetime in the region used in this analysis (see Fig. 4). Then, starting with p_T distributions at fixed charged multiplicity for the subset of events with $K^0_S(\Lambda^0)$ proper lifetime greater than 0.8×10^{-10} s ($1.0 \times 10^{-10} s$), the mean p_T is computed the same way as described in Sec. V and the difference between the mean p_T values for the full data set and the high τ subset is assigned as a systematic uncertainty for this correction. Since the correction is applied only to calculations of the mean p_T at fixed multiplicity and of the number of $K^0_S(\Lambda^0)$, the systematic uncertainty associated with it affects only these measurements. It amounts to about 6% (10%) for the total number of K^0_S (Λ^0) and affects the average number of $K^0_S(\Lambda^0)$ as a function of the charged multiplicity by the same amount. These systematic uncertainties combined in quadrature with the other systematic uncertainties discussed in this section are included in Figs. 11–16.

3. To investigate the systematic effect of the track reconstruction procedure on the efficiency correction, we compare our result with a set of MC events where the tracks are reconstructed using the CTC information alone, as opposed to the default SVX + CTC track reconstruction. We find that the variation on the final corrected p_T distribution is negligible.

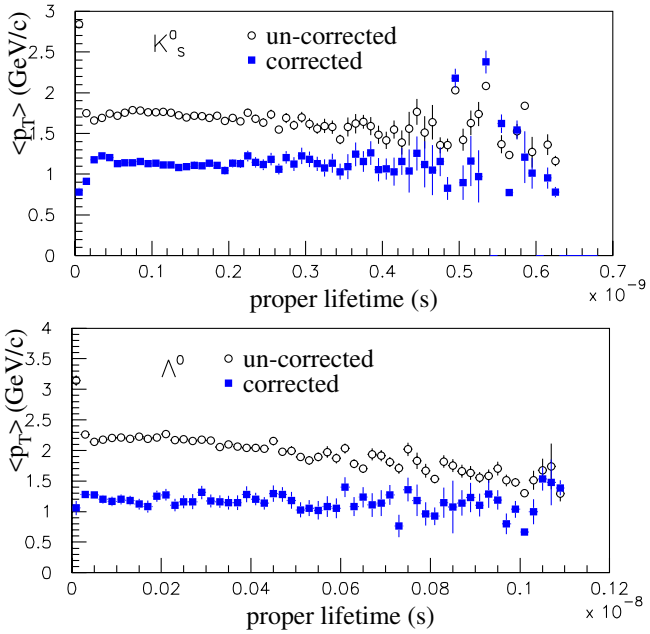

FIG. 4 (color online). The mean p_T of K^0_S and Λ^0 as a function of proper lifetime (t) at 1800 GeV. Raw and corrected data are shown.

4. Other sources of systematic uncertainties include the dependence of the results on the instantaneous luminosity and the uncertainty associated with the identification and selection of good isolated $p\bar{p}$ interactions from secondary or closely spaced event vertices (see [4]). The first may affect the results because higher luminosity gives higher detector occupancy which in turn can alter the V^0 identification. This has been investigated by analyzing data samples recorded at different instantaneous luminosities. The results show no observable effect. The second source can lead to incorrect event selection and produce associations of tracks that fake a V^0. This source has been investigated by comparing data samples with different requirements for a good $p\bar{p}$ vertex [4]. The results give systematic variations smaller than 9% on the overall number of $K^0_S(\Lambda^0)$.

5. The uncertainty on the correction is distributed in different ways for different observables. As a consequence, the integral of the corrected distribution of each variable is different. For example, the total number of $K^0_S(\Lambda^0)$ extracted from the integral of the corrected p_T distribution may be very different from that extracted from the multiplicity distribution. In particular, as discussed in the previous section, the p_T correction has been observed to be unreliable for $p_T \lesssim 0.7$ GeV/c where a large part of the V^0 cross section lies, so that the area under the distribution may be subject to large uncertainties. Given this, we use the global (integrated) correction from the PYTHIA MC as a correction factor for the total number of $K^0_S(\Lambda^0)$. We renormalize each distribution to this number to which we

TABLE II. Summary of all systematic uncertainties. For each systematic uncertainty source its effect on the various measured quantities is reported. The symbol "···" means no effect on the corresponding quantity.

Systematic uncertainty source	$\langle p_T \rangle$ vs mult. (included in figures)	p_T distr.	$N(V^0)$ distr. (not included in figures)	$\langle N(V^0) \rangle$ vs mult (not included in figures)	$N(V^0)$	K/π (included in Table IV)
MC simulation	3% (K^0_S) 4% (Λ^0)	10%	10–25%	2–20%	···	···
Low-p_T extrapolation	3–20%	···	5% (K^0_S) 10% (Λ^0)	5% (K^0_S) 10% (Λ^0)	5% (K^0_S) 10% (Λ^0)	6%
Primary vertex selection	···	···	<9%			
Global normalization factor	···	<30%				

attribute a 30% systematic uncertainty. This value is determined as the maximum difference that was found between the global corrected number of V^0 and the integral of any corrected distribution. Such uncertainty reflects on the K^0_S/π ratios and on the absolute scale of the ratios of the mean number of $K^0_S(\Lambda^0)$ to the charged multiplicity plotted in Figs. 17–20 .

Table II reports a summary of all the systematic uncertainties discussed.

VII. ANALYSIS RESULTS

A. Results

All data presented are subject to $p_T \geq 0.4$ GeV/c and $|\eta| \leq 1$ requirements, as specified in Sec. III, and are corrected for acceptance and vertex-finding efficiency. Systematic uncertainties are not included except where explicitly stated. Table I shows the raw and corrected numbers of $K^0_S(\Lambda^0)$ selected in our fiducial region for the full MB sample as well as for the *soft* and the *hard* samples. The corrected mean number of $K^0_S(\Lambda^0)$ per event in each sample is also shown; systematic uncertainties are included.

In Fig. 5 for the K^0_S and in Fig. 6 for the Λ^0, the normalized multiplicity of $K^0_S(\Lambda^0)$ for the MB, *soft*, and *hard* events is shown separately for the $\sqrt{s} = 1800$ GeV (solid symbols) and 630 GeV (open symbols) data. The probability of producing one or more Λ^0 is lower than the equivalent K^0_S probability, and the difference increases with V^0 multiplicity. This behavior is more pronounced in the *soft* subsample. The results shown in Figs. 5 and 6, with their statistical errors, are reported in Table III.

The invariant p_T inclusive distributions of K^0_S are shown in Figs. 7 and 8 at the two energies for the full MB, *soft*,

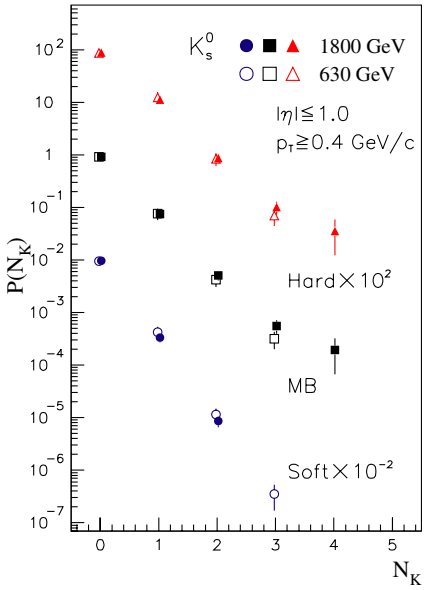

FIG. 5 (color online). Distribution of the multiplicity of K^0_S at 1800 (full symbols) and 630 GeV (open symbols).$P(N_K) =$ (number of events with $N_K K^0_S$)/(total number of events). MB, *soft* (divided by 100), and *hard* data (multiplied by 100) are shown.

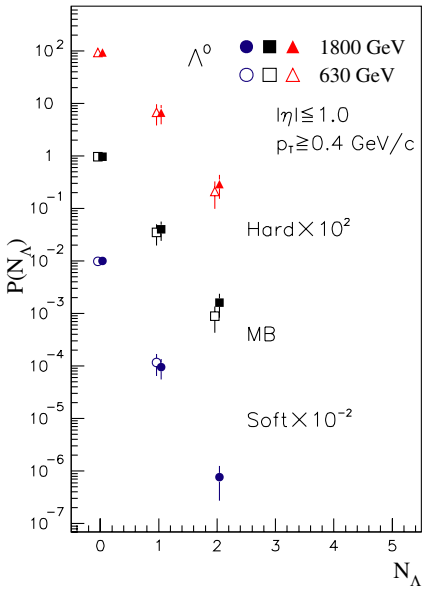

FIG. 6 (color online). Distribution of the multiplicity of Λ^0 at 1800 (full symbols) and 630 GeV (open symbols). $P(N_\Lambda) =$ (number of events with $N_\Lambda \Lambda^0$)/(total number of events). MB, *soft* (divided by 100), and *hard* data (multiplied by 100) are shown.

TABLE III. Number of events with N_K K^0_S (N_Λ Λ^0) divided by the total number of events. MB, *soft*, and *hard* data at 1800 and 630 GeV are reported.

	$N_{K/\Lambda}$	1800 GeV			630 GeV		
		MB ($\times 10^{-3}$)	Soft ($\times 10^{-3}$)	Hard ($\times 10^{-3}$)	MB ($\times 10^{-3}$)	Soft ($\times 10^{-3}$)	Hard ($\times 10^{-3}$)
K^0_S	0	919 ± 7	966 ± 2	880 ± 10	920 ± 10	956 ± 5	870 ± 20
	1	80 ± 10	33 ± 6	110 ± 20	80 ± 20	40 ± 10	120 ± 30
	2	5 ± 1	0.9 ± 0.2	9 ± 2	4 ± 1	1.2 ± 0.3	8 ± 2
	3	0.6 ± 0.2		1.0 ± 0.3	0.3 ± 0.1	0.04 ± 0.02	0.7 ± 0.3
	4	0.2 ± 0.1		0.4 ± 0.2			
Λ^0	0	958 ± 5	990.3 ± 0.1	930 ± 10	964 ± 5	988.3 ± 0.1	930 ± 10
	1	40 ± 20	10 ± 4	70 ± 30	40 ± 20	12 ± 5	70 ± 30
	2	1.6 ± 0.8	0.08 ± 0.05	3 ± 1	0.9 ± 0.5		2 ± 1

and *hard* samples. Data are normalized to the number of events in each sample. Figures 9 and 10 show the same p_T distributions for the Λ^0.

The dependence of the K^0_S and Λ^0 average p_T, calculated as described in Eq. (3), on the event charged multiplicity is shown in Figs. 11–13 (1800 GeV) and 14–16 (630 GeV). The mean p_T of primary charged tracks measured in the same phase space region, as published in [4], is also shown for comparison. For the K^0_S data set, in the region ranging from 0.4 to 0.8 GeV/c, the corrected data points are assumed to lay on a curve of form (2) extrapolated from the fit to the measured data points in the region $p_T >$ 0.8 GeV/c (details of the correction procedure are described in Sec. V). Note that, with the kinematical selection used in this analysis, no events with $p_T(\Lambda^0) < 1$ GeV/c were observed. For the measurement of $\langle p_T \rangle$, we fit the spectrum in the region of $p_T > 1.1$ GeV/c using Eq. (2) and extrapolate down to $p_T = 0.4$ GeV/c. We define the $\langle p_T \rangle$ as the mean value of the fitted function. This definition is adopted in order to compare the $\langle p_T \rangle$ with that of K^0_S and of charged tracks.

Figures 17–20 show the ratio of the mean number of $K^0_S(\Lambda^0)$ per event to the multiplicity as a function of the multiplicity itself. The charged particle multiplicity $N^\star_{\rm ch}$ was chosen as the reference variable to analyze V^0 production. The reason for this choice is based on the observation that the event charged multiplicity is a global event

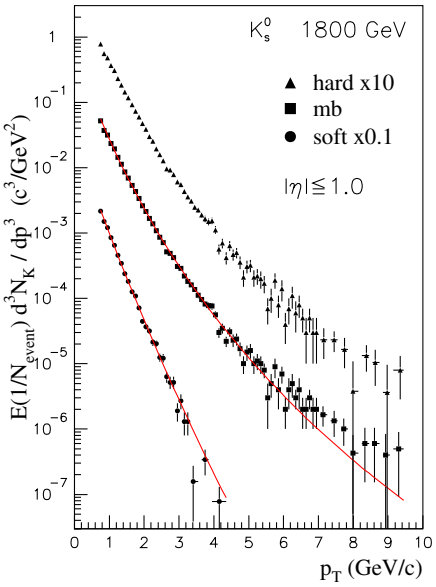

FIG. 7 (color online). K^0_S inclusive invariant p_T distributions at 1800 GeV. MB, *soft*, and *hard* data are shown, normalized to the number of events in each sample. E is the particle energy and $N_{\rm event}$ is the total number of events which contribute to the distribution. To separate the curves, *hard* data points are multiplied by 10 and *soft* data points by 0.1. The solid lines represent the best fits to Eq. (2) of the text.

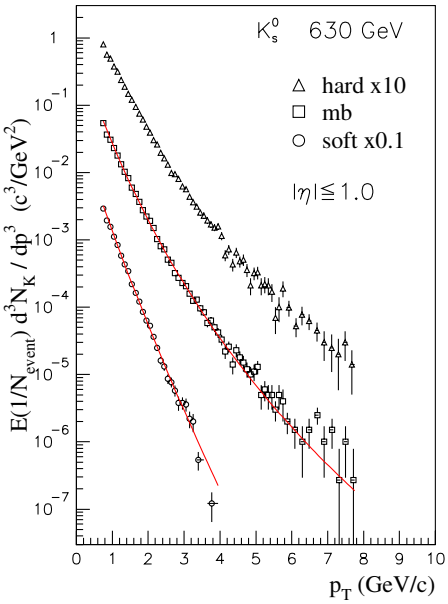

FIG. 8 (color online). K^0_S inclusive invariant p_T distributions at 630 GeV MB, *soft*, and *hard* data are shown, normalized to the number of events in each sample. E is the particle energy and $N_{\rm event}$ is the total number of events which contribute to the distribution. To separate the curves, *hard* data points are multiplied by 10 and *soft* data points by 0.1. The solid lines represent the best fits to Eq. (2) of the text.

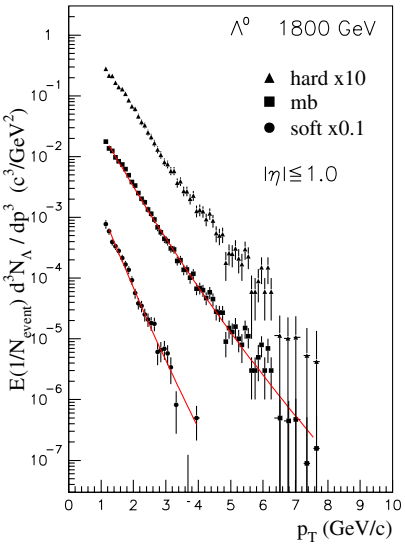

FIG. 9 (color online). Λ^0 inclusive invariant p_T distributions at 1800 GeV. MB, *soft*, and *hard* data are shown, normalized to the number of events in each sample. E is the particle energy and N_{event} is the total number of events which contribute to the distribution. To separate the curves, *hard* data points are multiplied by 10 and *soft* data points by 0.1. The solid lines represent the best fits to Eq. (2) of the text.

variable characterizing the whole multiparticle final state and is related to the hardness of the interaction (see [4,15,16]). As in the case of charged particles, possible new structures in the V^0 final state correlations would be

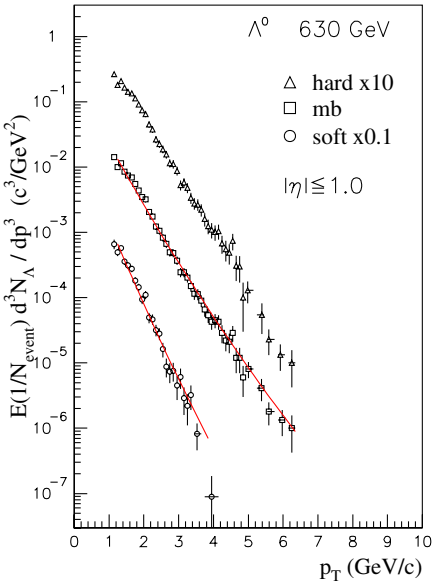

FIG. 10 (color online). Λ^0 inclusive invariant p_T distributions at 630 GeV. MB, *soft*, and *hard* data are shown, normalized to the number of events in each sample. E is the particle energy and N_{event} is the total number of events which contribute to the distribution. To separate the curves, *hard* data points are multiplied by 10 and *soft* data points by 0.1. The solid lines represent the best fits to Eq. (2) of the text.

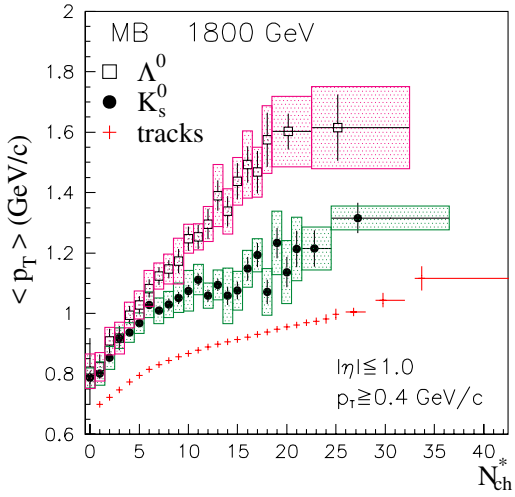

FIG. 11 (color online). Average transverse momentum $\langle p_T \rangle$ of K^0_S and Λ^0 at 1800 GeV as a function of the event charged multiplicity ($N^{\star}_{\text{ch}}$). MB data are shown. For comparison, the mean p_T of charged particles measured in the same phase space region is also plotted [4]. The filled squares around the points delimit the systematic uncertainties.

exhibited as a function of $N^{\star}_{\text{ch}}$. The dependence of the average p_T on multiplicity, for example, remains unexplained in any of the current models.

B. Dependence on E_T threshold

It has been remarked in the previous sections that the identification of *soft* and *hard* events is essentially a matter of definition. In order to investigate the sensitivity of the

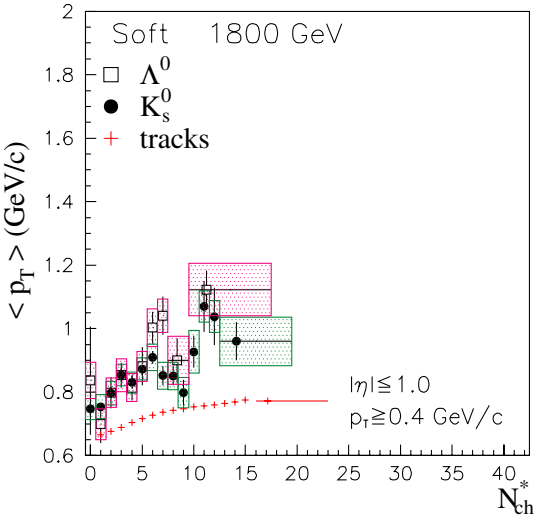

FIG. 12 (color online). Average transverse momentum $\langle p_T \rangle$ of K^0_S and Λ^0 at 1800 GeV as a function of the event charged multiplicity ($N^{\star}_{\text{ch}}$). *Soft* data are shown. For comparison, the mean p_T of charged particles measured in the same phase space region is also plotted [4]. The filled squares around the points delimit the systematic uncertainties.

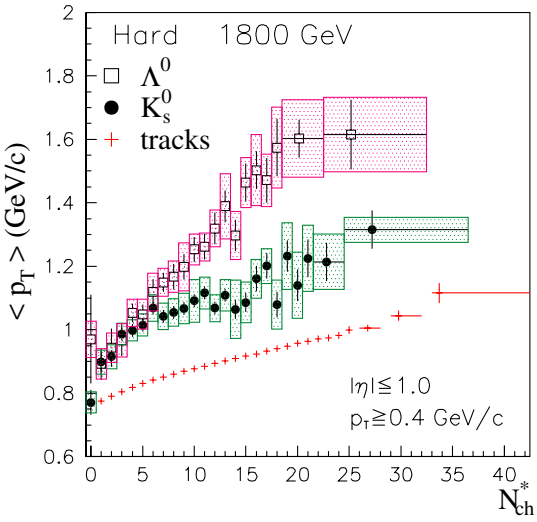

FIG. 13 (color online). Average transverse momentum $\langle p_T \rangle$ of K^0_S and Λ^0 at 1800 GeV as a function of the event charged multiplicity ($N^\star_{\rm ch}$). *Hard* data are shown. For comparison, the mean p_T of charged particles measured in the same phase space region is also plotted [4]. The filled squares around the points delimit the systematic uncertainties.

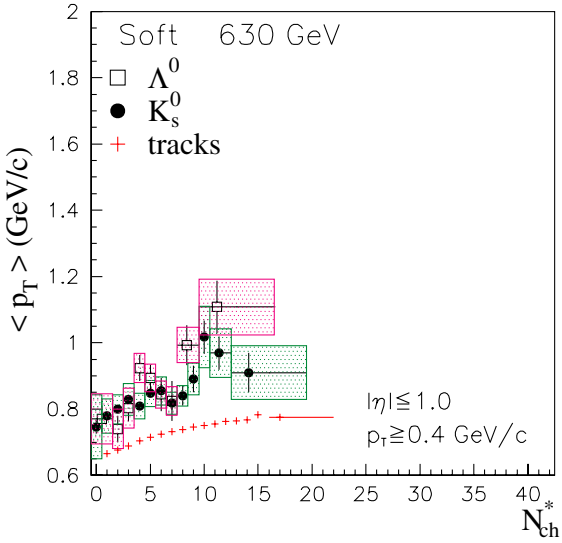

FIG. 15 (color online). Average transverse momentum $\langle p_T \rangle$ of K^0_S and Λ^0 at 630 GeV as a function of the event charged multiplicity ($N^\star_{\rm ch}$). *Soft* data are shown. For comparison, the mean p_T of charged particles measured in the same phase space region is also plotted [4]. The filled squares around the points delimit the systematic uncertainties.

above results to the cluster energy threshold used to separate *soft* and *hard* events, the analysis has been repeated changing the E_T threshold from 1.1 to 3.0 GeV. Although, as expected, the higher threshold value influences the global statistics of the *soft* and *hard* components, it preserves the shapes of the inclusive p_T distributions and the characteristics of the *hard* and the *soft* samples, and it does not change the shape of the correlations. With the new E_T threshold the fraction of K^0_S per event rises by the same

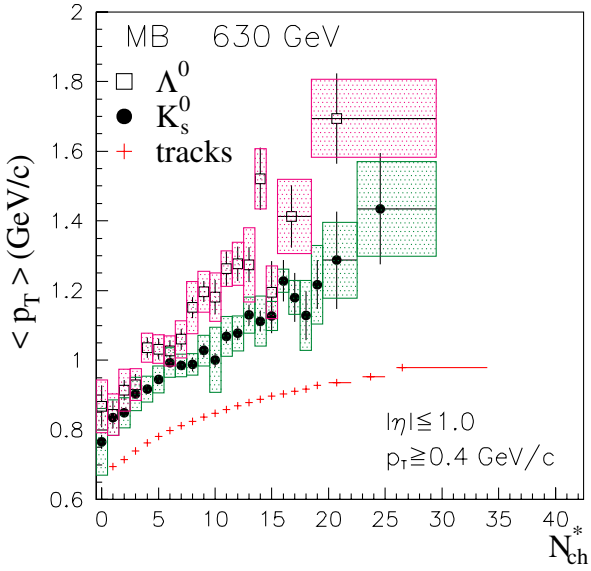

FIG. 14 (color online). Average transverse momentum $\langle p_T \rangle$ of K^0_S and Λ^0 at 630 GeV as a function of the event charged multiplicity ($N^\star_{\rm ch}$). MB data are shown. For comparison, the mean p_T of charged particles measured in the same phase space region is also plotted [4]. The filled squares around the points delimit the systematic uncertainties.

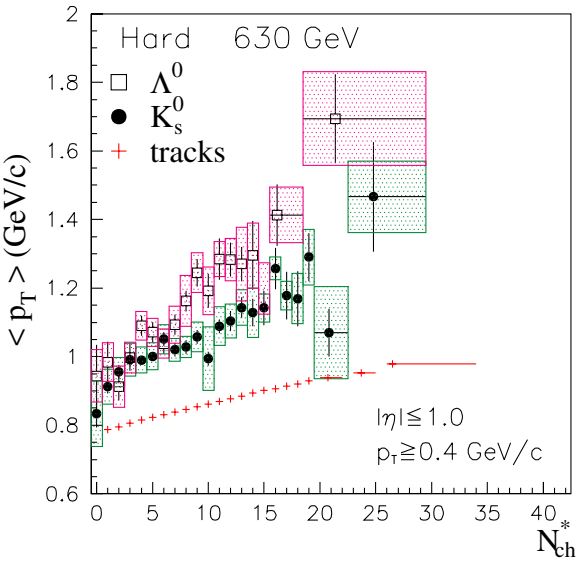

FIG. 16 (color online). Average transverse momentum $\langle p_T \rangle$ of K^0_S and Λ^0 at 630 GeV as a function of the event charged multiplicity ($N^\star_{\rm ch}$). *Hard* data are shown. For comparison, the mean p_T of charged particles measured in the same phase space region is also plotted [4]. The filled squares around the points delimit the systematic uncertainties.

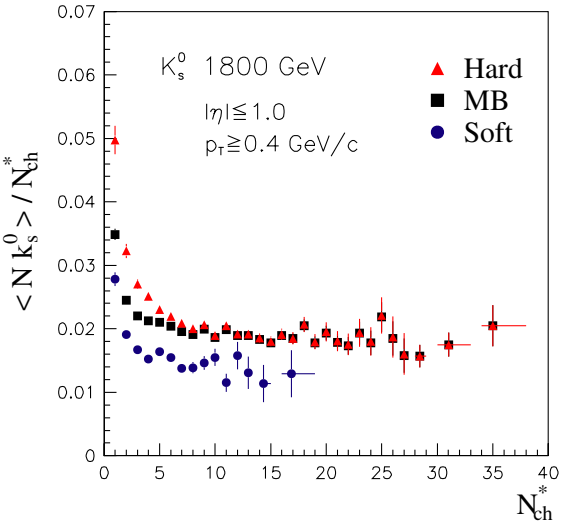

FIG. 17 (color online). Mean number of K^0_S per event divided by the charged multiplicity ($N^\star_{ch}$) and plotted as a function of $N^\star_{ch}$. The MB, *soft* and *hard* data at 1800 GeV are shown.

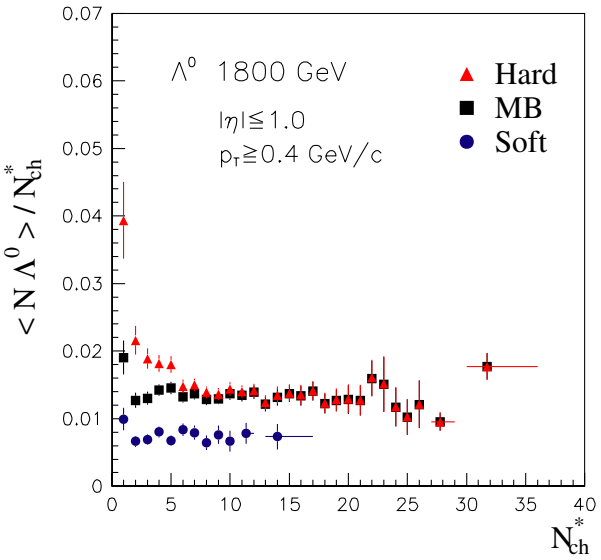

FIG. 19 (color online). Mean number of Λ^0 per event divided by the charged multiplicity ($N^\star_{ch}$) and plotted as a function of $N^\star_{ch}$. The MB, *soft*, and *hard* data at 1800 GeV are shown.

amount, around 30%, in the two samples. This means that the ratio of the rate of K^0_S in *soft* events to the same rate in *hard* events is not influenced by the higher threshold.

C. Analysis discussion

Some simple observations can be made about Table I. The fraction of the total K^0_S that falls into the *soft* subsample is rather small, ranging from about 30% at 630 GeV to about 18% at 1800 GeV (19% and 10% for Λ^0, respectively). The corrected mean number of K^0_S produced per event in the full MB sample is about $(8.6 \pm 2.6)\%$ at 630 GeV and $(8.8 \pm 2.6)\%$ at 1800 GeV (respectively, $(3.7 \pm 1.1)\%$ and $(4.3 \pm 1.0)\%$ for Λ^0).

The K^0_S/π cross-section ratio may be obtained by fitting the K^0_S and charged-track invariant p_T distributions in the available p_T range and extrapolating the fitted functions down to the minimum p_T value. This ratio is evaluated both for $p_{T\,\mathrm{min}} = 0$ GeV/c and $p_{T\,\mathrm{min}} = 0.4$ GeV/c. With the above technique, a ratio of 0.13 ± 0.04 (including the systematic uncertainty) at $\sqrt{s} = 1800$ GeV and 0.18 ± 0.05 at 630 GeV is obtained for $p_{T\,\mathrm{min}} = 0.4$ GeV/c. The

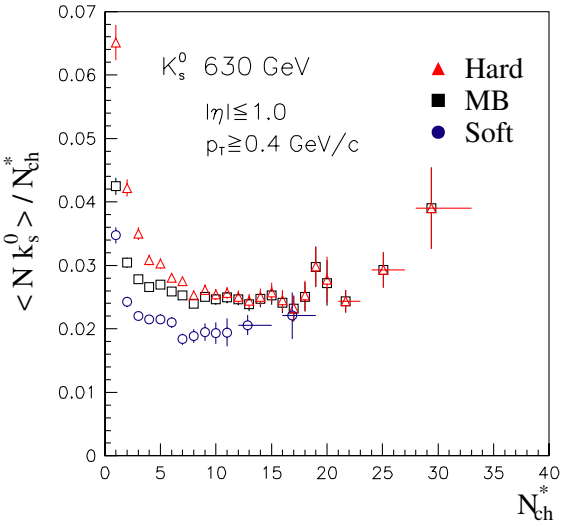

FIG. 18 (color online). Mean number of K^0_S per event divided by the charged multiplicity ($N^\star_{ch}$) and plotted as a function of $N^\star_{ch}$. The MB, *soft*, and *hard* data at 1800 GeV are shown.

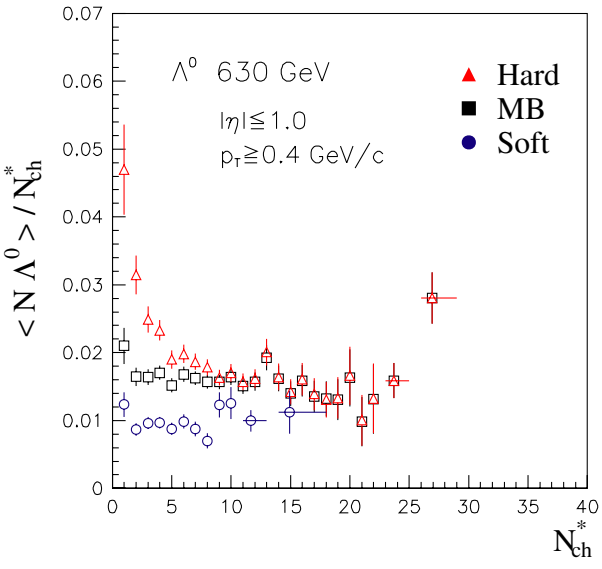

FIG. 20 (color online). Mean number of Λ^0 per event divided by the charged multiplicity ($N^\star_{ch}$) and plotted as a function of $N^\star_{ch}$. The MB, *soft*, and *hard* data at 630 GeV are shown.

TABLE IV. K^0_S/π ratio in each data set. Data computed in the full p_T range and for $p_T \geq 0.4$ GeV/c are shown. The ratios are evaluated integrating the p_T distributions by extrapolating the fitted function down to $p_{T\,\mathrm{min}} = 0.(0.4)$ GeV/c. Here efficiency corrections and systematic uncertainties are included.

	$p_{T\,\mathrm{min}}$ (GeV/c)	MB	Soft	Hard
1800	0.0	0.14 ± 0.05	0.38 ± 0.12	0.11 ± 0.04
	0.4	0.13 ± 0.04	0.30 ± 0.09	0.11 ± 0.03
630	0.0	0.19 ± 0.06	0.42 ± 0.13	0.14 ± 0.05
	0.4	0.18 ± 0.05	0.33 ± 0.10	0.18 ± 0.06

same ratio for $p_{T\,\mathrm{min}} = 0$ GeV/c gives 0.14 ± 0.05 at $\sqrt{s} = 1800$ GeV and 0.19 ± 0.06 at 630 GeV (Table IV). These last measurements are compatible with the previous CDF results [17], though slightly higher at $\sqrt{s} = 630$ GeV. In Table IV, the corresponding values for the *soft* and *hard* subsamples are reported. It is remarkable that the K^0_S/π ratio is about 2 times larger in *soft* than in MB events.

Studies of the production of strange particles K^0_S and Λ^0 in proton-antiproton interactions at different $\sqrt{s}$ are described in Ref. [18] at $\sqrt{s} = 540$ GeV and [19] at 200 and 900 GeV. In Refs. [17,20,21], results at $\sqrt{s} = 1800$ GeV are presented. Comparison with our results is restricted to the full MB samples; furthermore, it should be noted that here no absolute cross sections are provided. Comparison with Refs. [18–20] also requires taking into account the different p_T and η regions selected.

Figures 21–24 show a comparison of our data with MC. Corrected experimental data are compared with the PYTHIA generator (V6.216) in a configuration tuned to better match MB data. We refer to [4] for a description of the tuning. Generated events are not simulated through the apparatus but selected to match the acceptance limits imposed in the analysis. In these figures the invariant p_T distribution and the correlation of the average p_T with multiplicity are shown for K^0_S and Λ^0 at 1800 GeV. MC p_T distributions of K^0_S do not agree with data, in particular, in the low-p_T region. The number of K^0_S per event in PYTHIA is about 2.4 times larger than in data. The agreement is much better for Λ^0. The MC agreement with data for the correlation of $\langle p_T \rangle$ with the charged multiplicity is worse than for inclusive distributions. The $\langle p_T \rangle$ of generated K^0_S is systematically lower than data while that of Λ^0 is higher.

A direct comparison of the invariant p_T distribution of K^0_S can be done with Ref. [17]. There the p_T distribution of K^0_S is fitted to the functional power-law form of Eq. (2), fixing the parameter p^0 to 1.3 GeV/c. The average $\overline{p_T}$ is computed from the parameters of the fit as

$$\overline{p_T} = 2\frac{p^0}{n-3}. \tag{4}$$

With the new increased statistics and larger p_T range, the fit with the p^0 parameter fixed, while giving a reasonable description of the p_T spectrum in the low-p_T region, does not describe the data at higher p_T. It yields a $\overline{p_T}$ compatible with the previous one (see Table V) but with a large $\chi^2/N_{\mathrm{d.o.f.}}$. The best fit to our distribution (shown in

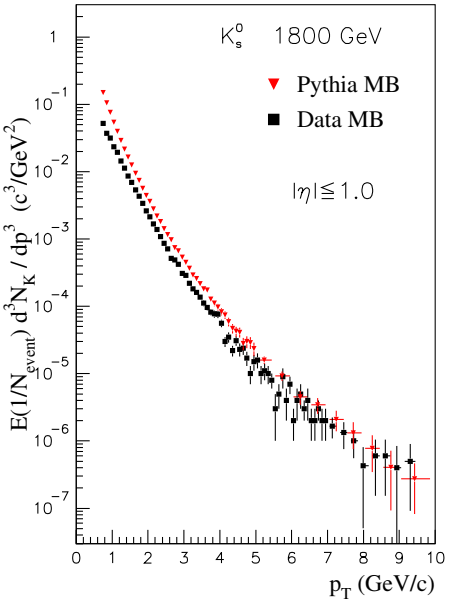

FIG. 21 (color online). K^0_S invariant p_T distribution in PYTHIA and data.

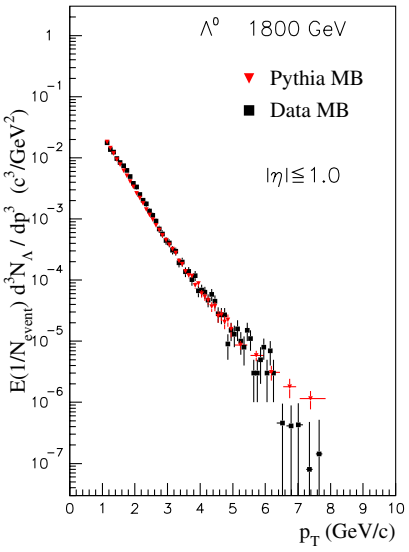

FIG. 22 (color online). Λ^0 invariant p_T distribution in PYTHIA and data.

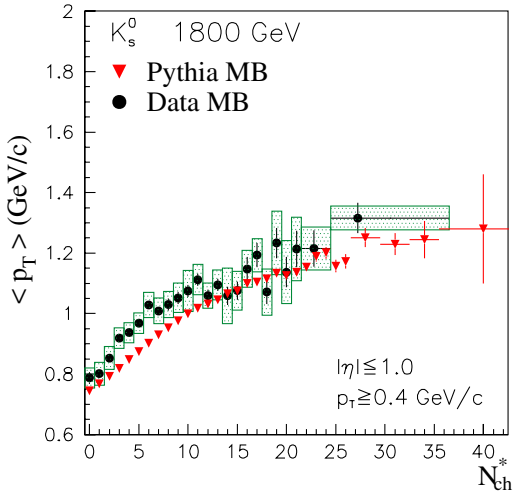

FIG. 23 (color online). Correlation of the average p_T of K^0_S with multiplicity in PYTHIA and data.

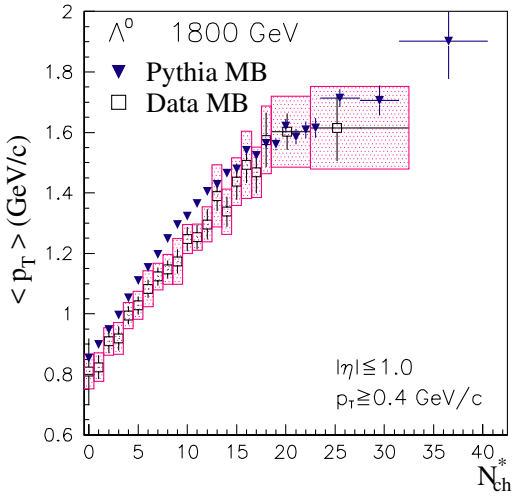

FIG. 24 (color online). Correlation of the average p_T of Λ^0 with multiplicity in PYTHIA and data.

Figs. 7–10 for the *soft* and MB samples) is obtained with this form when all three parameters are allowed to vary freely and the fit region is restricted to $p_T > 1$ GeV/c. A summary of the results is reported in Table V. The measurements reported in Refs. [18–21] were done at different energies and in different phase space regions.

From our best fit of MB sample data at 1800 GeV (630 GeV), the mean p_T of K^0_S is (0.75 ± 0.07) GeV/c [(0.70 ± 0.08) GeV/c]. These values are significantly higher than the previous CDF measurements due to the higher statistics in the high-p_T tail of the distribution.

Taking into account the different conditions and the method of measurement, it is possible to compare to UA5 data (Refs. [18,19]) as well; our present measurement is also higher in this case. For completeness, the fit results of the p_T invariant distribution for the *soft* subsample are also reported in Table V. A second fitting function used is of the form

$$E\frac{d^3N_k}{dp^3} = \exp(A + B\mathrm{p_T}), \quad \text{where } \overline{p_T} = -\frac{2}{B}\cdot \qquad (5)$$

At both energies, we obtain a good $\chi^2/N_{\mathrm{d.o.f.}}$ using this function (see Table V). Therefore, the shape of the *soft* distribution is also well described by an exponential function; the mean p_T of the fit is generally larger than what is obtained using Eq. (2). For Λ^0, a systematically higher mean p_T than other experiments at equivalent energy is obtained (compare with Refs. [19,20]). In this case as well, MB data can be equally well fitted by form (2) and by an exponential function. A summary of these results is in Table VI.

The increase of the mean p_T [computed as in Eq. (3)] of the observed K^0_S as a function of the event charged multiplicity is always larger than that of charged tracks. The increase for Λ^0 is even larger, leading to the conclusion that it depends on the particle mass, as expected. A similar

TABLE V. Results of the fit to the invariant p_T distribution of K^0_S. Data at different E_{cms} are reported (for different experiments the parameters of the fit were reported when available). Parameters p^0 and n refer to the power-law (P.L.) function [Eq. (2)], B to the exponential (Exp.) form [Eq. (5)]. CDF-0 refers to the so-called run-0 of the Tevatron [17] and CDF-I to run I data (this analysis).

Experiment ($\sqrt{s}$ in GeV)	Data set	$\overline{p_T}$ (GeV/c)	p^0 (P.L.) (GeV/c)	n (P.L.)	B (Exp.)	$\chi^2/N_{\mathrm{d.o.f.}}$
UA5 [a] (546)[18]	MB	0.58 ± 0.04	...	...		1.15
CDF-0 (630)[17]	MB	0.5 ± 0.1	1.3 (fixed)	7.9 ± 0.03		3.9
CDF-I (630)	MB	0.70 ± 0.08	3.3 ± 0.2	12.6 ± 0.6		68/57
UA5 [a] (900)[19]	MB	0.63 ± 0.03	...	...		0.5
CDF-0 (1800)[17]	MB	0.60 ± 0.03	1.3 (fixed)	7.7 ± 0.2		0.74
CDF-I (1800)	MB	0.58 ± 0.02	1.3 (fixed)	7.49 ± 0.02		265/68
CDF-I (1800)	MB	0.75 ± 0.07	3.29 ± 0.08	11.7 ± 0.1		67/67
CDF-I (630)	Soft	0.58 ± 0.04	9.0 ± 0.1	33.7 ± 0.1		29/22
CDF-I (630)	Soft	0.64 ± 0.02			-3.12 ± 0.03	24/23
CDF-I (1800)	Soft	0.62 ± 0.02	9.5 ± 0.3	33.7 ± 0.9		23/25
CDF-I (1800)	Soft	0.67 ± 0.02			-3.00 ± 0.04	29/26

[a]UA5 fits to a power-law form in $p_T > 0.4$ together with an exponential form in $p_T < 0.4$ GeV/c.

TABLE VI. Results of the fit to the invariant p_T distribution of Λ^0. Data at different $E_{\rm cms}$ are reported (for different experiments the parameters of the fit were reported when available). Parameters p^0 and n refer to the power-law (P.L.) function [Eq. (2)], B to the exponential (Exp.) form [Eq. (5)]. CDF-I refers to run I data (this analysis).

Experiment ($\sqrt{s}$ in GeV)	Data set	$\overline{p_T}$ (GeV/c)	p^0 (P.L.) (GeV/c)	n (P.L.)	B (Exp.)	$\chi^2/N_{\rm d.o.f.}$
UA5 (546)[18]	MB	0.62 ± 0.08	...	...		...
CDF-I (630)	MB	0.91 ± 0.07	12.3 ± 0.1	30.1 ± 0.2		59/35
CDF-I (630)	MB	0.98 ± 0.01			-2.05 ± 0.03	50/36
UA5 (900)[19]	MB	0.97 ± 0.01			...	...
CDF-I (1800)	MB	0.97 ± 0.09	12.4 ± 0.1	28.6 ± 0.09		41/45
CDF-I (1800)	MB	1.04 ± 0.01			-1.92 ± 0.02	55/46
CDF-I (630)	Soft	0.67 ± 0.09	10.0 ± 0.2	33.0 ± 0.2		31/24
CDF-I (630)	Soft	0.73 ± 0.1			-2.74 ± 0.05	28/25
CDF-I (1800)	Soft	0.64 ± 0.05	9.5 ± 3.3	33.0 ± 0.2		29/22
CDF-I (1800)	Soft	0.73 ± 0.10			-2.74 ± 0.05	25/23

analysis is also reported in Ref. [21]. A direct comparison is not possible because of the different p_T range and η acceptance, which reflect in larger multiplicities. However, a rise in mean p_T with heavier particle masses is clearly observed.

In the analysis of charged tracks [4], all the correlations examined in the MB and in the *hard* samples showed different behaviors with respect to $E_{\rm cms}$, while a clear invariance was seen in the *soft* sample. With the available $K^0_S(\Lambda^0)$ statistics it is not possible to discern any difference in the $\langle p_T \rangle$ dependence on multiplicity at the two energies, even in the full MB sample. Nevertheless, the behavior of the three subsamples is clearly different. We note that the mean $K^0_S(\Lambda^0)$ p_T increases with $N^\star_{\rm ch}$ also in the *soft* subsample, a feature that is not explained by the current models [2,4,15,16,22]. This observation also holds for charged hadrons, as discussed in [4].

The ratios of the mean numbers of $K^0_S(\Lambda^0)$ per event to the charged multiplicity drop in the first few bins ($0 \lesssim N^\star_{\rm ch} \lesssim 6$) and are roughly constant for $N^\star_{\rm ch} \geq 6$ (MB sample) for both K^0_S and Λ^0. The dependence on $N^\star_{\rm ch}$ is more pronounced for K^0_S than for Λ^0. The fraction of Λ^0 per event and per track is obviously smaller than that of K^0_S and for both is larger at 630 GeV than at 1800 GeV. Finally, the dependencies of the number of Λ^0 for the *soft* and the MB samples on $N^\star_{\rm ch}$, besides differing by about a factor of 2, are both roughly flat and different in shape from the corresponding K^0_S distributions.

VIII. CONCLUSIONS

The present measurements extend the studies of charged particle properties in MB $p\bar{p}$ interactions to K^0_S and Λ^0 production. Using the data available at the two c.m.s. energies obtained under the same experimental conditions and similar statistics, we are able to directly compare the V^0 production properties at the two c.m.s. energies. Our results offer new findings and significant improvements to the existing knowledge of V^0 production. We summarize our results as follows:

(i) The overall production rates of K^0_S and Λ^0 are in agreement with previous measurements.

(ii) The inclusive p_T spectra of K^0_S and Λ^0 now extend to $p_T \geq 8$ GeV/c. The K^0_S distribution shows a more detailed shape in the high-p_T region when compared to previous data. For both K^0_S and Λ^0, we measure an average p_T significantly higher than previous results.

(iii) New results are presented on the distribution of K^0_S and Λ^0 multiplicity.

(iv) For the first time, the MB sample has been used to analyze V^0 production properties in its *soft* and *hard* components. Inclusive p_T and multiplicity distributions of V^0 are shown for the *soft* and *hard* data.

(v) Analyses of the dependence of the mean $K^0_S(\Lambda^0)$ p_T with the event charged multiplicity are presented. Comparison with an analogous study performed on charged tracks indicates that the rate of the dependence grows with particle mass. An increase of the mean p_T is observable also in the *soft* subsample alone.

(vi) The observed dependence is not explained by the current theoretical models. A comparison with PYTHIA confirms this observation. A better agreement with data is obtained for the inclusive p_T distributions.

(vii) The event charged multiplicity has been adopted as the independent variable to analyze the ratio of the mean number of $K^0_S(\Lambda^0)$ per event to the number of primary charged particles. For both K^0_S and Λ^0 this ratio rises toward very low multiplicity, remaining roughly constant for $N^\star_{\rm ch} \gtrsim 5$.

ACKNOWLEDGMENTS

We thank the Fermilab staff and the technical staffs of the participating institutions for their vital contributions. This work was supported by the U. S. Department of Energy and National Science Foundation; the Italian

Istituto Nazionale di Fisica Nucleare; the Ministry of Education, Culture, Sports, Science and Technology of Japan; the Natural Sciences and Engineering Research Council of Canada; the National Science Council of the Republic of China; the Swiss National Science Foundation; the A. P. Sloan Foundation; the Bundesministerium fuer Bildung und Forschung, Germany; the Korean Science and Engineering Foundation and the Korean Research Foundation; the Particle Physics and Astronomy Research Council and the Royal Society, UK; the Russian Foundation for Basic Research; the Comision Interministerial de Ciencia y Tecnologia, Spain; in part by the European Community's Human Potential Programme under Contract No. HPRN-CT-2002-00292; and the Academy of Finland.

[1] R. Ansari *et al.*, Z. Phys. C **36**, 175 (1987); X. Wang and R. C. Hwa, Phys. Rev. D **39**, 187 (1989); F. Ceradini (UA1 Collaboration), in *Proceedings of the International Europhysics Conference on High Energy Physics, Bari, 1985* (Laterza, Bari, 1985).
[2] T. Sjöstrand and M. van Zijl, Phys. Rev. D **36**, 2019 (1987), and references therein.
[3] A summary of the references to these models can be found in [2].
[4] D. Acosta *et al.*, Phys. Rev. D **65**, 072005 (2002).
[5] F. Abe *et al.*, Nucl. Instrum. Methods Phys. Res., Sect. A **271**, 387 (1988), and references therein.
[6] F. Abe *et al.*, Phys. Rev. D **52**, 4784 (1995).
[7] F. Bedeschi *et al.*, Nucl. Instrum. Methods Phys. Res., Sect. A **268**, 50 (1988).
[8] F. Snider *et al.*, Nucl. Instrum. Methods Phys. Res., Sect. A **268**, 75 (1988).
[9] F. Balka *et al.*, Nucl. Instrum. Methods Phys. Res., Sect. A **267**, 272 (1988); S. R. Hahn *et al. ibid.* **267**, 351 (1988); K. Yasuoka *et al. ibid.* **267**, 315 (1988); R. G. Wagner *et al. ibid.* **267**, 330 (1988); T. Devlin *et al. ibid.* **268**, 24 (1988); S. Bertolucci *et al. ibid.* **267**, 301 (1988); Y. Fukui *et al. ibid.* **267**, 280 (1988); S. Cihangir *et al. ibid.* **267**, 249 (1988); G. Brandenburg *et al. ibid.* **267**, 257 (1988).
[10] As we do not distinguish Λ^0 from $\bar{\Lambda}^0$, in this paper Λ^0 stands for both.
[11] K. Hagiwara *et al.* Particle Data Group, Phys. Rev. D **66**, 010001 (2002); Phys. Rev. D **66**, 010001 (2002).
[12] F. Abe *et al.*, Phys. Rev. D **56**, 3811 (1997); Phys. Rev. Lett. **79**, 584 (1997); X. Wang, Phys. Rev. D **46**, R1900 (1992); C. Albajar *et al.* (UA1 Collaboration), Nucl. Phys. **B309**, 405 (1988).
[13] T. Sjöstrand, Comput. Phys. Commun. **82**, 74 (1994); G. Marchesini, B. R. Webber, G. Abbiendi, I. G. Knowles, M. H. Seymour, and L. Stanco, Comput. Phys. Commun. **67**, 465 (1992).
[14] G. Arnison *et al.*, Phys. Lett. B **118**, 167 (1982); F. Abe *et al.*, Phys. Rev. Lett. **61**, 1819 (1988).
[15] L. Van Hove, Phys. Lett. B **118**, 138 (1982); R. Hagedorn, Riv. Nuovo Cimento **6**, 10 (1984); J. D. Bjorken, Phys. Rev. D **27**, 140 (1983).
[16] X. Wang and C. Hwa, Phys. Rev. D **39**, 187 (1989); M. Jacob, CERN Report No. CERN/TH. 3515, 1983 (to be published); F. W. Bopp, P. Aurenche, and J. Ranft, Phys. Rev. D **33**, 1867 (1986).
[17] F. Abe *et al.* (CDF Collaboration), Phys. Rev. D **40**, 3791 (1989).
[18] K. Alpgard *et al.* (UA5 Collaboration), Phys. Lett. B **115**, 65 (1982); G. J. Alner *et al.* (UA5 Collaboration), Nucl. Phys. **B258**, 505 (1985).
[19] R. E. Ansorge *et al.* (UA5 Collaboration), Phys. Lett. B **199**, 311 (1987).
[20] S. Banerjee *et al.* (E735 Collaboration), Phys. Rev. Lett. **62**, 12 (1989).
[21] T. Alexopoulos, in *Proceedings of II International Conference on Physics and Astrophysics of Quark-Gluon Plasma, Calcutta, 1993* (World Scientific, River Edge, NJ, 1994).
[22] S. Barshay, Phys. Lett. B **127**, 129 (1983).